ELSEVIER

Biophysical Chemistry 68 (1997) 109–125

Biophysical Chemistry

Infrared spectroscopy: a new frontier in medicine

Michael Jackson, Michael G. Sowa, Henry H. Mantsch *

Institute for Biodiagnostics, National Research Council, Winnipeg, Manitoba, Canada R3B 1Y6

Abstract

As we enter the second half of the nineties, one of the major challenges for biological infrared spectroscopists is to transfer the knowledge we have gained from studies on isolated molecules to the complex world of medicine. That it is possible to meet this challenge is suggested by comparison with the development of other biophysical techniques, such as magnetic resonance spectroscopy and imaging, which have already found their place in medical research and practice. The Spectroscopy Group in Winnipeg is developing and evaluating a variety of new IR techniques for the analysis of body fluids and tissues, both in vitro and in vivo. Herein, we review these methodologies, which comprise both instrumental (imaging and spatially localized IR spectroscopy) and interpretational procedures aimed at optimizing the measurements and their conversion to biodiagnostic information. © 1997 Elsevier Science B.V.

Keywords: Molecular medicine; Infrared spectroscopy; Infrared imaging; Medical diagnosis

1. Historical perspective

In 1800, the British astronomer Sir William Herschel discovered the infrared region of the electromagnetic spectrum, paving the way for the rapid development of the technique of infrared spectroscopy [1]. Within 35 years, the first mid infrared spectrometer had been constructed [2], and within about 90 years the technique was finding applications in astronomy (for example, examining the emission spectrum of the sun [3]) and in physical [4], organic [5] and atmospheric chemistry. [1] The success of spectroscopic techniques in these areas led the prominent physiologist Thomas Huxley to comment "What an enormous revolution would be made in biology, if physics or chemistry could supply the physiologist with a means of making out the molecular structures of living tissues comparable to that which spectroscopy affords to the inquirer into the nature of the heavenly bodies". Although Huxley did not know it, physicists and chemists had already provided the physiologist with just such a means, in the form of infrared spectroscopy. This was amply demonstrated by the pioneering work of Blout and Mellors [7] and Woernley [8], who demonstrated that infrared spectra of human and animal tissues could indeed provide information concerning the molecular structure of the tissue. Unfortunately, this avenue of exploration was not vigorously pursued, perhaps due to the complexity of both the systems under investigation and the spectra they produced as well as instrumental limitations. Instead, attention was focused on the spectroscopic properties of isolated

* Corresponding author.

[1] S.P. Langley (1881), cited in Ref. [6].

biological molecules, particularly proteins, lipids and nucleic acids.

The demonstration by Elliot and Ambrose [9,10] that the major protein absorption in IR spectra is sensitive to protein conformation was followed by almost 50 years of successful infrared spectroscopic analysis of protein structure [11–14]. For about 30 years, IR spectroscopy has been used to probe lipid/membrane structure and dynamics, providing more information relating to lipid phase behaviour than almost any other physical technique [15–17]. Furthermore, many investigators have taken advantage of the fact that lipid–protein interactions can be studied by IR spectroscopy, and information relating to both the lipid and protein components extracted [18,19]. Unfortunately, nucleic acids have not been studied as extensively as lipids and proteins, but IR spectroscopy has still provided much valuable information, particularly respecting transitions between the various structural forms of DNA [20,21].

We now have 50 years of experience with infrared spectroscopic studies of isolated biological materials. In addition, significant advances in instrumentation and data processing have been made which allow an unprecedented amount of information to be recorded and then decoded from IR spectra. With this in mind, it seemed appropriate to us to revisit the use of infrared spectroscopy in the study of tissues, applying the results of these 5 decades of fruitful research to further our understanding of the spectroscopic properties of tissues. In this article, we will review the methodologies which we have developed over the last 5 years for the characterisation of tissues and the diagnosis of disease states. For convenience, we divide our studies into three distinct but related areas: IR pathology, IR clinical chemistry and IR imaging. The power of infrared spectroscopy in tissue characterisation and disease diagnosis will be illustrated with representative examples from each of these areas.

2. Definitions and methodologies

2.1. Definitions

The definition of infrared clinical chemistry is quite straight forward: it is the infrared spectroscopic analysis of biological fluids resulting in the quantitative determination of analytes of interest. The infrared spectroscopic approach to clinical chemistry has two important advantages when compared to classical clinical chemistry techniques. First, no reagents are required. Many of the standard clinical chemistry tests require the addition of reagents to the sample to produce a coloured product and the concentration of the product is determined colourimetrically. This approach is necessary as relatively few naturally occurring biological species have strong, characteristic UV or visible spectra. On the other hand, all of the organic and many of the inorganic materials present in biological fluids give rise to infrared spectra without the need for chemical modification.

As with all other forms of optical spectroscopy, the intensity of IR absorptions arising from a particular species is directly proportional to the concentration of that species. In addition, as infrared spectroscopy is an averaging technique, all infrared active components are probed simultaneously. Thus, the infrared spectrum of a biological fluid is the sum of the absorptions arising from all of the IR active species present in the fluid, weighted according to the concentration of each species. This leads to the second major advantage of IR clinical chemistry: as the IR spectrum of a biological fluid is the sum of all of the IR active components present in the fluid, the concentration of each IR active component is encoded in each spectrum. Thus, in principle, it is possible to determine the concentration of multiple analytes from a single spectrum, imparting a significant saving of time and labour.

We define infrared pathology as the study of the disease process by infrared spectroscopic analysis of excised tissue and isolated cells. Again, this approach has a number of advantages over the classical approach to pathology. For instance, fixation and staining of tissues are necessary before a histological assessment of tissue sections can be performed. No fixation or staining is required for IR studies. Indeed, staining is undesirable as the stain will itself contribute significantly to the infrared spectrum of the sample. Fixation may also result in artefactual results if care is not exercised in the choice of fixative. Furthermore, an IR spectroscopic approach to pathology has the major advantage that it provides infor-

mation concerning the molecular structure of the tissue.

2.2. Spectral acquisition techniques

Infrared clinical chemistry measurements may take a variety of forms, including standard transmission measurements conducted on the native biological fluid. However, the strong molar absorptivity of water in the mid infrared region of the spectrum can cause serious problems unless the measurement is restricted to very short pathlengths (< 10 μm). Such short pathlengths lead to problems with reproducibility. Problems associated with strong water absorptions may be overcome by drying the fluid to form a film, making measurements in the near infrared or using specialised techniques such as attenuated total reflectance (ATR) spectroscopy. ATR methods are not without problems (including adsorption of materials onto the ATR substrate and a dependence of penetration depth upon wavelength which causes spectral distortions), and we prefer to make measurements on dry films in the mid infrared [22] or on the native fluid in the near infrared [23]. Both methods have the advantage that very small volumes of fluid are needed, 10–20 μl for mid infrared investigations of films and 200–300 μl for near infrared investigations of the native fluid.

Sampling methods for infrared pathology are more numerous than for infrared clinical chemistry. Any cell suspension or tissue found in the body can be analysed by infrared spectroscopy if sufficient sample can be obtained and the appropriate sampling technique is available. The definition of 'sufficient' depends upon the instrumentation available to the investigator. For standard transmission experiments conducted between infrared transparent windows, high quality spectra can be obtained from cell suspensions containing 10–50,000 cells, depending upon the size of the cells. In the case of tissues, such measurements generally require a sample size of 1 mm^3. If an infrared microscope is available, spectra may be obtained from single cells if the cells are larger than 10 μm in diameter. With smaller cells, spectra may be obtained from clusters of 5–10 cells. In the case of tissues, the infrared microscope allows thin sections (10 μm) to be analysed with a very high spatial resolution (10 μm $\times$ 10 μm).

Many samples are more difficult to analyse, and cannot be easily sectioned with a microtome or pressed between windows. Examples of such samples include bone and teeth. Bone can be de-mineralised to soften the sample and allow sectioning. However, if the crystallinity of the mineral phase (or even the amount of different minerals present) is of interest, then this approach is unfeasible. Instead, techniques such as diffuse reflectance or photoacoustic spectroscopy may be used. An additional advantage of photoacoustic spectroscopy is that with the use of a step-scan interferometer depth profiling can be performed, providing information concerning compositional/structural changes with increasing depth of penetration of the IR radiation [24].

2.3. Data processing techniques

Once spectra have been obtained, there are a number of data processing methods available to extract qualitative and quantitative information. The first method we apply is the classical approach to spectroscopic data analysis, often referred to as the group frequency approach. Using this approach, particular absorptions are assigned to various functional groups in an attempt to extract biochemical information from the spectra. For example, absorptions between 1620–1680 cm^{-1} are usually attributed to the amide I vibration of proteins, while absorptions at 1080 and 1240 cm^{-1} are attributed to the PO_2^- symmetric and asymmetric stretching vibrations of DNA phosphodiester groups [25]. Using such assignments, qualitative and semi-quantitative information can be extracted from spectra.

Quantitative information can be obtained from IR spectra using a number of data processing methods. The simplest method consists of measuring the integrated area of an absorption band of interest and correlating the intensity of this marker band with the concentration of the analyte under investigation. Such a method can only be applied if the marker band is well resolved (i.e., does not overlap with any other absorptions). Such a situation is unfortunately rare in biological samples and the method is not generally applicable. However, one example is described below (Sections 3.1 and 3.2).

In most cases where quantitative information is required, the absorptions arising from the analyte of

interest show significant overlap with absorptions from other species. In such cases, methods such as partial least squares analysis can be calibrated to correlate complex changes in reference spectral signatures with changes in analyte concentration [26]. This calibrated method can then be used to predict analytes in unknown samples. Occasionally, it is possible to simplify the analysis by simplifying the question. For example, rather than knowing the absolute concentration of an analyte, it may be sufficient simply to know if the analyte is present or not. An automated multivariate pattern recognition method such as linear discriminant analysis (LDA) can then be trained to recognise the complex spectroscopic features characteristic of the presence or absence of the analyte.

Multivariate pattern recognition methods are powerful tools for the comparison of a large number of variables within a data set (hence, the term, multivariate). Variables include the absolute intensity of one or more absorptions, the position of one or more absorptions, the relative intensities of two or more absorptions, the width of one or more absorptions, the relative width of two or more absorptions, and so on. Multivariate pattern recognition methods can then determine patterns in these variables which are characteristic of subsets of the data (hence, the term, pattern recognition). For a complex data set, it may be that a combination of 10 or more variables is required to adequately determine a pattern which is characteristic of a particular subset.

Multivariate pattern recognition techniques fall into two general classes: unsupervised and supervised. Unsupervised methods such as hierarchical clustering determine intrinsic structure within data sets, without prior knowledge. With such methods, a direct comparison of spectra is made and subsets of data formed based upon spectral similarities. Supervised methods such as LDA are generally more powerful tools, and make use of the fact that the investigator often has a substantial amount of information available regarding the data set. This information may be, for example, biochemical or clinical in nature. This information is used to train the pattern recognition algorithm to recognise the particular combination of variables in a subset of data which is characteristic of the information. The algorithm can then search for this combination of variables in test data and make a classification based upon its presence or absence. Application of techniques such as LDA and cluster analysis have allowed us to classify IR spectra of isolated cells, tissues and biological fluids and diagnose a variety of disease states with a high degree of accuracy [22,23,27].

The application of these data acquisition and processing techniques is illustrated in the following sections.

3. Infrared clinical chemistry

3.1. Quantitation of thiocyanate in saliva

Saliva is perhaps the most easily obtained biological fluid, which has led to many attempts to find a diagnostic use for this complex material. The most successful of these attempts led to the development of a method for the diagnosis of cystic fibrosis based upon the concentration of NaCl in saliva. While simple inorganic materials such as NaCl cannot be analysed by infrared spectroscopy, other materials present in saliva give rise to strong, characteristic absorptions. These material include proteins, lipids, carbohydrates and thiocyanate. Thiocyanate is converted to the potent antibacterial compound hypothiocyanite, and possibly plays a role in preventing infection of the oral cavity by opportunistic bacteria. Thiocyanate is also present in the body as a by-product of cigarette smoking, and thiocyanate levels have been investigated extensively as a possible indicator of smoking status.

Infrared spectra of films formed by drying saliva under a light vacuum show many absorptions which are found in all biological fluids, which may be attributed to the lipid (2800–3000 cm^{-1}), protein (3300, 1650 and 1550 cm^{-1}) and carbohydrate (1000–1200 cm^{-1}) components of saliva (Fig. 1). In addition, a well resolved band arising from thiocyanate is apparent at 2058 cm^{-1}, a spectral region fortunately devoid of absorptions in most biological systems [28]. Dry protein films prepared from solutions enriched in thiocyanate also show this absorption, suggesting that thiocyanate in saliva films is complexed with proteins (interestingly, we have also shown that metabolically produced CO_2 trapped in dry films of biological fluids also appears to be

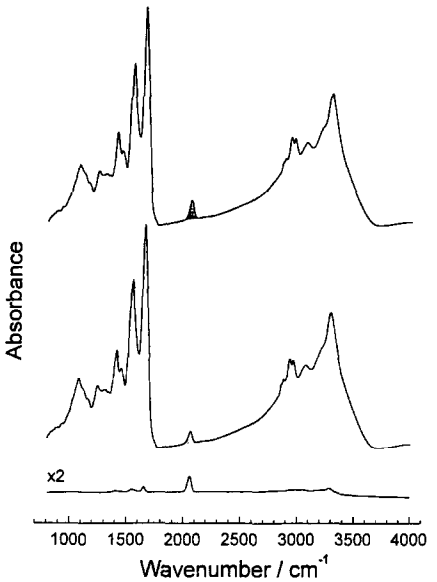

Fig. 1. IR spectra of dry films of human saliva collected in the morning (upper trace) and late afternoon (middle trace) from the same individual. The lower trace is the difference spectrum generated by subtraction of the middle trace from the upper trace. The thiocyanate absorption at 2058 cm^{-1} is shaded.

complexed with proteins [29]). The integrated intensity of the thiocyanate absorption in protein films and the added thiocyanate concentration were linearly related (Beer's law), with a calibration coefficient of 0.994 (Fig. 2). Assuming the molar absorptivity of the thiocyanate–protein complex in protein films is similar to that seen in saliva, the thiocyanate concentration in saliva samples could then be determined. In particular, the variation in saliva thiocyanate throughout the day was investigated (Fig. 1). The results indicated that thiocyanate concentrations peak early in the morning (2.7 mM) and decrease throughout the day, levelling of at 0.7 mM by late afternoon [27].

The advantages of this infrared spectroscopic approach compared to more traditional methods for thiocyanate determination (colourimetry and HPLC) include simplicity, speed and the fact that expensive reagents are not required.

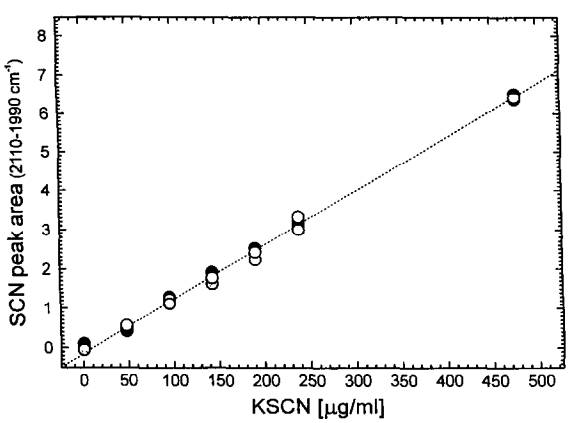

Fig. 2. Integrated area of the thiocyanate absorption at 2058 cm^{-1} in dry protein films as function of added KSCN concentration. Each measurement was made in triplicate. The inset shows the thiocyanate absorptions at each concentration.

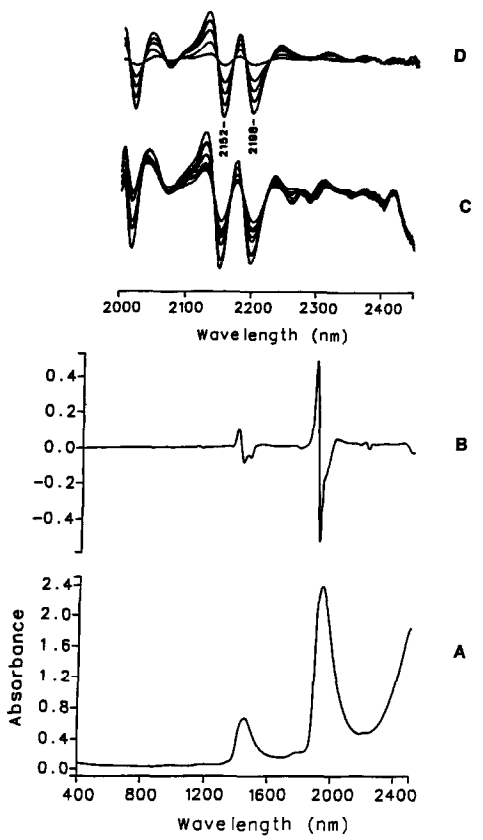

Fig. 3. Near infrared spectra of urine and urea. (A) Original absorbance spectrum of urine. (B) Second derivative spectrum of urine. (C) Expanded second derivative spectra of 10 urine samples. (D) Expanded second derivative spectrum of urea at 5 concentrations.

3.2. Quantitation of analytes in urine

Analysis of urine has been of fundamental importance in medicine for centuries. Of particular importance from a clinical point of view are urine glucose, protein, urea and creatinine concentrations. Currently, these analytes are determined colourimetrically using an automated clinical chemistry analyser. While highly precise and accurate, this method has the disadvantage of being expensive of reagents and can only be used for determination of one analyte at a time. We have investigated the potential use of near infrared spectroscopy for the determination of urine protein, creatinine and urea [30].

The near infrared spectrum of urine is presented in Fig. 3 (traditionally, near IR spectra are presented in nm rather than wavenumbers). As expected, the spectrum is dominated by broad absorptions from water. Calculation of the second derivative of the absorbance spectrum reveals a number of weaker absorptions which arises from solutes dissolved in the urine (Fig. 3B,C). Comparison with the second derivative spectrum of urea solutions demonstrates that many of these weak absorptions can be attributed to urea (Fig. 3D). As absorptions from urea are the major solute absorptions, it is relatively straight forward to develop a calibration for urea concentration based upon a correlation between spectral intensities and measured urea concentration using Beer's law. The urea absorption at 2152 nm provides the best calibration, resulting in a linear relationship between intensity and measured urea concentration with a slope of close to unity [30]. The accuracy of this calibration was verified by prediction of the urea concentration in a number of unknown samples, which were then analysed by standard laboratory methods. Again, a linear relationship was found between urea concentrations determined by the near infrared and standard methods, with a slope close to unity (Fig. 4). This simple approach can therefore be used to accurately quantitate urea concentrations in urine. A more flexible model which simultaneously examined fluctuations in other absorption bands resulted in slightly improved accuracy [30].

The absorptions arising from creatinine and proteins are much weaker than those arising from urea, and are overlapped by absorptions from other species. Partial least squares analysis is the most appropriate prediction method in this case. Using reference spec-

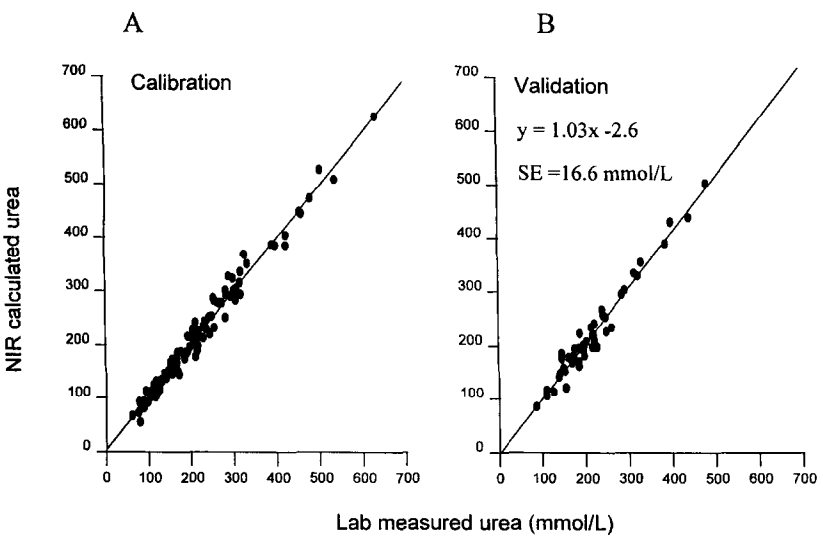

Fig. 4. Determination of urea concentration in urine using near infrared spectroscopy. (A) Calibration curve calculated for spectra of urine samples with known urea concentrations. (B) Regression of urea concentration predicted from spectra of unknown urine samples against actual values. SE = standard error of prediction.

tra and experimentally determined analyte concentrations, PLS methods derive factors from spectra which account for spectral variance. This variance may be due to spectral noise, baseline shifts or directly related to changes in analyte concentrations. Extraction of the factors correlated with variance in the analyte of interest allows a linear relationship between concentration and spectral properties to be determined, which then forms the basis of the calibration for that analyte. Using this approach, a linear relationship between experimentally determined urine creatinine concentrations and concentrations determined by near infrared spectroscopy was found, with a slope of 0.953 [30]. For protein determination, the slope of the relationship between lab values and near infrared values was lower, 0.923, implying a reduced accuracy for protein concentration determination by near infrared spectroscopy.

As with quantitation of thiocyanate ion concentration, the advantages of the infrared clinical chemistry approach to urine analysis are the lack of reagents, simplicity and speed.

3.3. Prediction of foetal lung maturity

A major problem in the management of high risk pregnancies is the determination of foetal lung maturity. This determination is required in order for the attending physician to be able to determine whether or not the lungs are sufficiently developed to allow unassisted breathing if labour must be induced prematurely. If the lungs are not sufficiently mature, a condition known as respiratory distress syndrome (RDS) results, which even when not fatal, can result in significant long term health problems. For unassisted breathing to occur, the foetal lung must be able to produce sufficient surfactant, of correct composition, to reduce the surface tension in the alveoli and allow expansion of lung following parturition. The lung is considered to be mature when the ratio of lecithin to sphingomyelin, two major components of lung surfactant, in the amniotic fluid reaches a value of two.

The lecithin to sphingomyelin ratio (L/S ratio) is most commonly assessed by thin layer chromatographic analysis of amniotic fluid samples obtained by amniocentesis. While TLC is the gold standard for the assessment of L/S ratios world-wide, it is not without drawbacks. Drawbacks include a large coefficient of variation and the length of time the analysis requires. This has led to the search for alternative techniques for the determination of the L/S ratio.

As lipids have highly characteristic infrared spectra, we decided to investigate the potential use of infrared spectroscopy for the determination of L/S ratios [31]. We have used partial least squares (PLS) regression analysis to correlate the intensity of absorbances arising from sphingomyelin and lecithin in near infrared spectra of amniotic fluid with the L/S ratio determined by TLC. A linear correlation between the L/S ratio predicted from near infrared spectra and the ratio determined by TLC is obtained, with a correlation coefficient of 0.91, demonstrating that this near infrared spectroscopic method can be used to reliably determine the L/S ratio in amniotic fluid samples.

4. Infrared pathology

4.1. Characterisation of leukaemic lymphocytes and diagnosis of leukaemia

Disease states resulting from disturbances of the biochemistry of the cellular elements of blood are tempting targets for spectroscopic study as they can be easily obtained in a pure, concentrated form. This has prompted us to begin an investigation of the spectroscopic properties of leukaemic lymphocytes [32]. Representative infrared spectra of films of lymphocytes from a control subject and a subject with chronic lymphocytic leukaemia (CLL) are shown in Fig. 5. These complex spectra arise from the super imposition of the individual spectra of all of the infrared active constituents of the cells, including lipids, proteins, nucleic acids and carbohydrates. Despite the complexity of the spectra, it is possible to assign absorptions in some spectral regions to vibrations of specific chemical groups within individual cellular components. Absorptions from proteins dominate the spectral regions between 1500–1700 cm^{-1} (polypeptide N–H bending and C=O stretching vibrations, while the region between 1000–1300 cm^{-1} and 1400–1500 cm^{-1} are dominated by absorptions from nucleic acid phosphodiester PO_2^- stretching

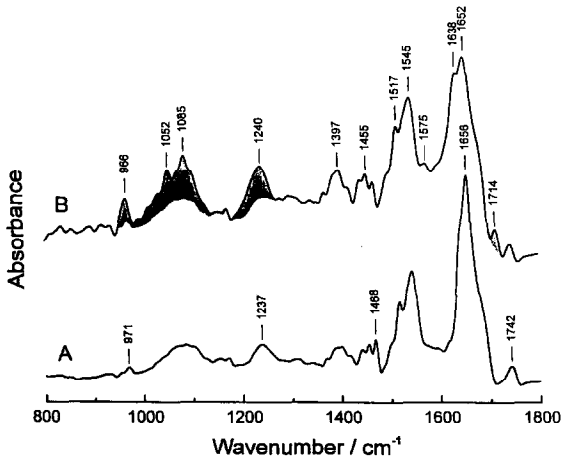

Fig. 5. Deconvolved infrared spectra of control (A) and leukaemic (B) lymphocytes. Shaded areas illustrate spectral differences attributed to differences in nucleic acids.

vibrations and phospholipid acyl chain CH_2 and CH_3 bending vibrations, respectively.

The frequency and relative intensity of these absorptions provides structural and quantitative information. For example, the frequency of the absorption arising from the polypeptide backbone C=O stretch (1620–1680 cm^{-1}, known as the amide I band) is sensitive to the secondary structure of the proteins present. Furthermore, the frequency of the CH_2 and CH_3 bending and stretching absorptions are sensitive to packing constraints within cell membranes, while the frequency of the phosphodiester PO_2^- stretching vibrations are sensitive to hydrogen bonding interactions within nucleic acids. The intensity of each absorption is directly proportional to the concentration of the relevant chemical group present in the sample. If the structure/interactions and/or concentrations of cellular lipids, proteins or nucleic acids is altered in CLL, an analysis of the positions and relative intensities of the major absorptions seen in control and CLL cells should provide information concerning the nature of the biochemical changes accompanying leukaemia, which should also prove to be diagnostic spectral markers.

A comparison of the control and CLL lymphocyte spectra shown in Fig. 5 reveals a number of important differences [32]. The ratio of the intensity of the amide I band to the intensity of the CH_2 stretching absorptions is increased in CLL cells (not shown), suggesting an increase in the protein content of the cells, a decrease in the lipid content or both. A decrease in the lipid content of CLL cells is also suggested by the reduction in the intensity of the absorptions at 1468 cm^{-1} (attributed to CH_2 bending vibrations) and 1742 cm^{-1} (attributed to lipid ester C=O stretching vibrations).

Significant changes in the shape of the protein absorptions are apparent. The frequency of the amide I maximum is shifted from 1656 cm^{-1} in control cells to 1652 cm^{-1} in CLL cells and there is a significant increase in intensity at 1636 cm^{-1}. Both of these changes are indicative of either gross structural modification of a large number of cellular proteins, a change in the relative concentrations of the cellular proteins (i.e., preferential expression of certain proteins) or the expression of a new set of proteins with different structural properties. In particular, the increased intensity at 1636 cm^{-1} in spectra of CLL cells indicates an increased proportion of β-sheet secondary structures. Gross structural modification of a significant number of cellular proteins seems unlikely, as this will result in a high proportion of non-functional proteins, leading to cell death. The shift in the amide I absorption therefore suggests a change in protein expression in CLL cells, with CLL cell proteins being rich in β-sheet secondary structures.

In addition to changes in the membrane lipids and cell proteins, significant differences are apparent in the PO_2^- stretching absorptions of the phosphodiester groups of nucleic acids. Differences are apparent in both the shape and intensity of the PO_2^- symmetric (1085 cm^{-1}) and asymmetric (1240 cm^{-1}) stretching vibrations, indicating that CLL cells have a greater nucleic acid content than control cells, and that the hydrogen bonding interactions of the nucleic acids are different in the two cell types. Increased nucleic acid content is also suggested by the increased intensity of the absorption at 1714 cm^{-1} in CLL cells, which arises from C=O stretching vibrations of nucleotide bases.

In addition to allowing diagnosis of CLL, infrared spectral features are also useful prognostically. Progressive changes in DNA content of CLL cells from a number of patients were spectroscopically detected over the course of 12 months, as deduced from a

progressive increase in the intensity of the absorption at 1714 cm^{-1}. Clinically, this correlates with a short lymphocyte doubling time in these patients. In other words, changes in the intensity of the absorptions attributed to DNA in CLL cells over time can be correlated with the degree of aggressiveness of the disease.

4.2. Characterisation of breast tumour tissue and staging of breast cancer

Characterisation of breast tissue provides a much greater challenge to the infrared spectroscopist than characterisation of lymphocytes, due to the difference in the nature of the samples. As discussed above, lymphocytes are tempting targets for study as they can easily be obtained as a pure suspension. In contrast, the epithelial cells of the breast, the component of breast tissue which is transformed in breast cancer, are anchored in a complex matrix consisting primarily of adipose tissue and collagen. This matrix of adipose tissue and collagen is not homogeneous and varies spatially and temporally, a fact which has important spectroscopic consequences [25].

A strong lipid content in breast tissue gives rise to intense absorptions at 1095, 1163, 1378, 1466, 1740 and 2800–3050 cm^{-1}, attributed to CO–O–C asymmetric and symmetric stretching, CH_3 symmetric bending, CH_2 bending, ester C=O stretching and CH_2 and CH_3 symmetric and asymmetric stretching vibrations respectively (Fig. 6A). A strong collagen component results in the appearance of absorptions at 1033, 1082, 1204, 1240, 1280 and 1338 cm^{-1}, arising from C–OH stretching absorptions of collagen carbohydrate moieties, C–N stretching vibrations of the collagen polypeptide backbone and CH_2 wagging vibrations of collagen side chains (Fig. 6B). In addition, a strong amide I absorption at 1634 cm^{-1} is apparent in spectra of collagen rich tissue. It can therefore be appreciated that the normal spatial and temporal variations in collagen and lipid content of breast tissue samples will result in major variations in almost all regions of the spectrum.

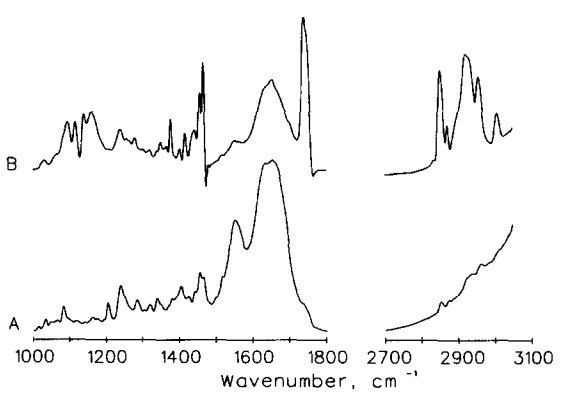

Fig. 6. Deconvolved infrared red spectra of human breast tumours with high collagen (A) and adipose tissue (B) content.

With such large variations in the spectral characteristics of breast tissue arising as a result of normal variations in breast tissue composition, can the much less pronounced changes expected as a consequence of the progression of the disease be detected? Many of the spectral changes expected to accompany disease progression may be masked by variations in lipid and/or collagen content. For example, as discussed above our studies on CLL have shown that the spectroscopic differences between normal and malignant lymphocytes include differences in the PO_2^- absorptions of DNA phosphodiester groups [32]. Unfortunately, these absorptions are seen at 1080 and 1240 cm^{-1}, regions of the spectrum dominated by absorptions from both collagen and lipid in breast tissue. Thus, changes in cellular DNA which accompany the disease process (e.g., altered chromosomal structure, increased DNA content) will be masked by the large changes in collagen and lipid content which occur between and within breast tumours. Similarly, changes in protein expression which accompany the disease process and are manifested in changes in the amide I absorption will be masked by differences in collagen content, while changes in cell membrane properties which would be manifested as changes in CH stretching absorptions will be masked by differences in lipid content. Visual discrimination of spectroscopic changes associated with the disease process in the breast is therefore unfeasible.

With visual discrimination of the spectral changes associated with breast cancer impossible, we applied sophisticated pattern recognition methods to the classification of breast tumour spectra [33]. Tumours were classified pathologically as high, intermediate or low grade. A linear discriminant algorithm was

trained to recognise the spectral features characteristic of each grade and 77 breast tumour spectra were classified. The results of this classification are shown in Table 1. Numbers in rows represent the results of histopathological classification of the tumours, while numbers in columns represent the classification predicted by the trained LDA algorithm. Numbers on the diagonal (in bold italics) show the number of correctly classified spectra. Thus, for 21 tumours pathologically classified as low grade, 19 (90.5%) gave rise to spectra which could be correctly classified as arising from low grade tumours. For intermediate grade tumours, the accuracy of the LDA classification was significantly reduced, only 26 of 34 spectra (76.5%) were correctly classified. In fact, perhaps not surprisingly, the accuracy of the LDA classification of the intermediate grade tumours was lowest of the three classifications attempted. It is interesting, however, that the analysis always misclassified intermediate grade tumours as high grade tumours, and never as low grade tumours. All high grade tumours were correctly classified. The overall accuracy of the method was 87%, with 67 of 77 tumours correctly classified [33].

In addition to grading tumours, we also attempted to use LDA to predict whether oestrogen and progesterone receptors were present in tumours. For oestrogen receptors, correct classification as either receptor positive or negative was achieved for 93.3% of tumours, with classification of oestrogen negative tumours being superior to classification of receptor positive tumours (88.9% vs. 96.3%). This situation was reversed for progesterone receptors, with 95.8% of receptor positive tumours being correctly classified compared to 84% of receptor negative tumours, and the overall accuracy of prediction was slightly reduced (89.8%). Obviously, this analysis is not detecting the presence of these receptor per se (steroid hormone receptor concentrations in the breast are of the order of fg/mg tissue) but is, we believe, detecting the spectroscopic consequences of the cascade of events initiated by receptor activation, such as protein phosphorylation.

Table 1
Results of linear discriminant analysis classification of breast tumour spectra by grade

	L	I	H	% Accuracy	SP (%)	PPV (%)
L	***19***	1	1	90.5	100	100
I	0	***26***	***8***	76.5	97.6	94.1
H	0	0	***22***	100	85.9	77.9

Overall accuracy = 87%.
Numbers in rows represent the pathological classification of tumours, results in columns are the calculated classifications. L = low grade, I = intermediate grade, H = high grade. Bold italics indicate correct classifications. See text for more details.

These results demonstrate that while spectra of breast tumours are complex, and innate variations in sample histology on a microscopic and macroscopic appear to mask spectral changes associated with the disease process, a surprising amount of clinically relevant information can be obtained by the correct application of multivariate pattern recognition methods.

4.3. Characterisation of Alzheimer's disease tissue

One of the major pathological hallmarks of Alzheimer's disease (AD) is the presence of neuritic plaques, neurotoxic aggregates of A4β amyloid peptide, in the grey matter of affected individuals. As aggregated proteins and peptides have characteristic infrared spectroscopic signatures [14], we attempted to identify the spectroscopic signature of A4β in AD tissue. Our initial studies focused on analysis of small pieces (1 mm^3) of AD tissue placed between IR transparent (diamond) windows. Although we could not reliably identify spectral features attributable to neuritic plaques, we could classify spectra as arising from control or AD tissue using LDA, hierarchical clustering and artificial neural networks with an impressive degree of success [27]. We ascribed our inability to identify spectral features due to neuritic plaques predominantly to two facts. Firstly, the method of analysis destroys the physical integrity of the tissue. It is therefore impossible to determine pathologically whether or not the tissue actually contained neuritic plaques. Secondly, even if neuritic plaques are present, the volume of plaques present in 1 mm^3 of tissue will be negligible compared to the volume of the tissue. The spectral information arising from the plaques will therefore be masked by the spectral features of the surrounding tissue, and it requires sophisticated pattern recognition techniques to decode this information.

The failure of this macroscopic approach to identify features characteristic of neuritic plaques in AD tissue led us to apply infrared microspectroscopy to the investigation of AD tissue [34]. Thin sections (10 μm) of AD grey matter were mounted on CaF_2 windows. An area of one section showing a dense amorphous deposit identified as a potential neuritic plaque was chosen for investigation. Using a variable aperture system, all tissue outside an area 12×12 μm was masked off. The IR spectrum of this area was then obtained, and the computer-controlled stage moved 12 μm. A second spectrum was acquired and the process repeated until spectra had been obtained from the whole area of interest. In this manner, a spectroscopic map of the tissue was generated with a spatial resolution of 12×12 μm. A 3 dimensional plot of the integrated intensity of the amide I absorption as a function of position was then generated (Fig. 7A). Analysis of this plot shows that there is a dramatic increase in the integrated intensity of the amide I band in the centre of the area mapped, corresponding exactly to the amorphous deposit of interest. This observation implies that the amorphous deposit is proteinaceous in composition. However, it does not allow any conclusions concerning the structure of the protein(s) in the deposit to be drawn. A plot of the centre of gravity of the amide I absorption as a function of position is shown in Fig. 7B. Blue colouration corresponds to an amide I absorption characteristic of β-sheet proteins (~ 1630 cm^{-1}), while orange/red coloration corresponds to an amide I absorption characteristic of unordered and/or helical proteins ($\sim 1650 - 56$ cm^{-1}). The area corresponding to the proteinaceous deposit can clearly be seen to exhibit a low amide I frequency (1630 cm^{-1}). Inspection of the deconvolved spectral data for this area of the tissue section reveals an amide I peak frequency at 1628 cm^{-1}, indicative of aggregated protein (not shown). Thus, our microspectroscopic data indicates that the amorphous mass observed in this microtomed section of AD grey matter consists of aggregated protein and may be a neuritic plaque. Subsequent staining of the tissue with Congo red, a stain which specifically colours amyloid deposits pink/red, revealed that the mass was indeed a neuritic plaque, confirming our spectroscopic observations (Fig. 7C).

Our studies on AD tissue have demonstrated that although a macroscopic spectroscopic approach coupled with pattern recognition techniques can be used to reliably distinguish between AD and control tissue, a microscopic approach is required to characterise the pathological hallmarks of the disease in situ.

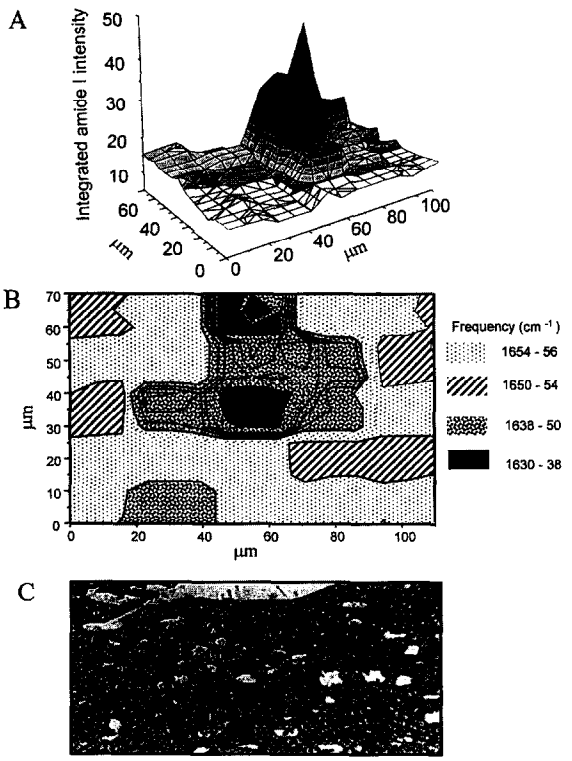

Fig. 7. Infrared microscopy of Alzheimer's disease grey matter. (A) Three dimensional surface map of the integrated intensity of the amide I band corresponding to the area marked in 7C. (B) Two dimensional contour map of the amide I peak frequency of the region mapped. (C) Enlarged photomicrograph of the tissue after staining with Congo red to show amyloid deposits. The rectangular box bounds the area mapped.

5. In vivo infrared imaging and spectroscopy

5.1. Background

Because of the high extinction coefficient throughout the infrared region of the electromagnetic

spectrum, the spectroscopy of living tissues in situ is problematic over much of that spectroscopic region. It is only at the red end of the visible spectrum and over the high energy near infrared region that the penetration depth of the radiation in tissue exceeds 1 mm. Despite this limitation, in vivo near infrared spectroscopy and imaging has considerable promise as a medically relevant diagnostic tool. The area of in vivo spectroscopy which has the longest history and greatest clinical relevance, to date, is the non-invasive measurement of haemoglobin oxygen saturation.

Prior to the development of the spectroscope, it was observed that the reaction of oxygen with haemoglobin increases the transmission of red light through solutions of haemoglobin and blood. Early spectroscopic investigations not only measured this increased transmission across the red end of the visible spectrum but also determined that transmission was generally decreased in the infrared region. In addition, certain (isobestic) wavelength regions where revealed at which the transmission was unaffected by the degree of haemoglobin oxygen saturation [35]. These early results indicated that the differential absorption of oxy- and deoxy-haemoglobin in the visible and near infrared could be used to measure the relative concentration of these species in blood. This approach was rapidly extended to in vivo measurements of haemoglobin oxygen saturation and resulted in published accounts as early as the 1930s and 1940s [36–38].

Pulse oximetry, developed in the 1970s [39], represented the next major evolution in in vivo monitoring. Real-time measurement of the differential attenuation of visible and infrared light in viable tissue consists of two-components; one component of the attenuation is modulated by the pulsation of blood, while the larger underlying attenuation is unaffected by pulsatile flow. The pulse modulated attenuation primarily arises from the arterial compartment. Thus, by excluding the underlying static attenuation and using only the pulse modulated component of the attenuation, the absorption arising from the surrounding tissue and venous blood are largely discriminated against. The differential attenuation of the pulse modulated component of the visible and infrared light in tissue therefore provides a measure of the arterial haemoglobin oxygen saturation (SaO_2), which can be empirically related or calibrated against the measured SaO_2 in arterial blood.

Pulse oximetry has a proven track record of providing a reliable measure of trends in haemoglobin oxygen saturation, noninvasively, in humans [40–42]. It has largely replaced methods which required a discrete blood sample and has thus enabled real-time non-invasive monitoring of SaO_2 in patients under anaesthesia or under intensive care. The clinical success of pulse oximetry suggests that other infrared spectroscopic based patient monitoring methods may be of clinical value.

5.2. Challenges facing non-invasive haemodynamic monitoring

Along with haemoglobin oxygen saturation, there are a number of blood related parameters that are of clinical interest. These haemodynamic parameters include, haematocrit (red blood cell concentration), blood volume and blood flow. In addition to monitoring trends in these haemodynamic parameters, a quantitative assessment of these parameters would be clinically useful, and considerable effort has been made to use near infrared spectroscopy to track haemodynamic parameters [43–49].

Several reports have used forearm occlusion protocols to demonstrate the potential of near infrared spectroscopy to monitor various haemodynamic parameters in a localized region of peripheral tissue. Recently, we have re-examined the spatial, temporal and spectral evolution of changes in the near infrared attenuation of the forearm under conditions of rapidly changing blood-flow, attenuated or arrested blood flow and under conditions of rapidly changing blood volume, using near infrared imaging and spectroscopy in conjunction with multivariate data analysis methods [50,51].

Fig. 8 illustrates the results for two experimental conditions. Each experimental condition manipulates the blood flow to the forearm. In the first experiment, blood flow to the lower forearm and hand is completely arrested (ischaemia) by application of 200 mm Hg pressure with a blood pressure cuff. In the second experiment the venous return of blood from the lower forearm and hand is impeded (venous occlusion) using a reduced pressure (100 mm Hg). In the case of forearm ischaemia, forearm blood volume

remains relatively constant while cellular metabolism alters the haemoglobin oxygen saturation and perturbs the redox status of cytochrome aa_3. During venous occlusion, forearm blood volume increases markedly, while the restricted blood return results in the accumulation of metabolites.

Near infrared reflectance images of the forearm were collected using a 512 × 512 pixel charge coupled device imaging system which makes use of a liquid crystal tunable filter to select the reflectance at particular near infrared wavelengths. The reflectance of the forearm at rest was normalised to zero to account for any uneven illumination of the surface. The change in the forearm reflectance over the period of occlusion was recorded at each pixel of the image. The most similar pixel time courses were determined by cluster analysis using a fuzzy C-mean clustering algorithm [52,53]. Fig. 8 reports the results

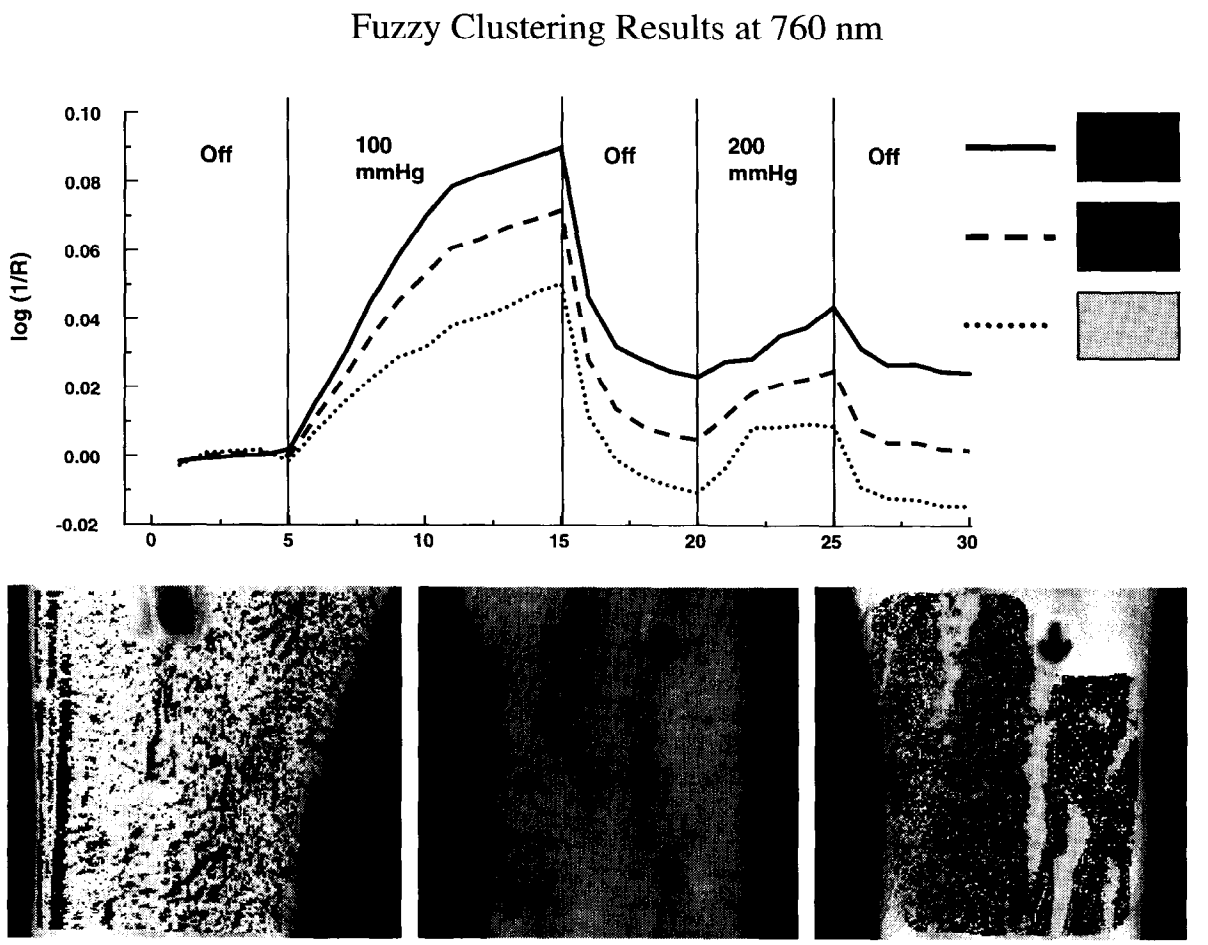

Fig. 8. Fuzzy clustering results, cluster centroid time courses and cluster membership maps, of the change in the reflectance response of the forearm at 760 nm during a forearm occlusion protocol. Top: Pixel cluster centroids of the 760 nm reflectance time courses during a forearm occlusion protocol which includes a 5 min period of venous occlusion (100 mm Hg pressure) and a 2.5 min period of complete forearm ischaemia (200 mm Hg pressure). Bottom: Anatomical forearm image (centre) and the 760 nm pixel time course clustering images (cluster membership maps) of the venous occlusion segment of the protocol (left) and the results from a complete forearm ischaemia protocol (right).

from the reflectance image time-series taken at 760 nm for a forearm occlusion protocol which included a 5 min period of venous occlusion and a 2.5 min period of complete ischaemia. The cluster centroid time courses are plotted in the upper panel. Cluster membership maps for ischaemia and venous occlusion are overlayed on the anatomical image of the forearm in the bottom right and bottom left panels of Fig. 8, respectively. The bottom centre image shows the visible/anatomical image of the forearm. As apparent from the visible image, features at several millimeters depth can be resolved by the imaging system.

During the venous occlusion segment of the protocol, each pixel in the sequence of near infrared reflectance images of the forearm displays a similar time-course, corresponding to an increase in the attenuation of reflected near infrared light with venous occlusion time. Clustering pixel reflectance time courses of greatest similarity enables regional variations in the tissue response to venous occlusion to be mapped. Differences in the magnitude of the attenuation between clusters during venous occlusion can be noted from the cluster centroid time courses. The cluster membership maps indicate the regional variations in this response across the forearm. The regional variations identified in the cluster membership maps are diffusely distributed across the forearm and do not clearly identify distinct anatomical features or regions. This is to be expected. The gross change in the overall blood volume in the forearm and hand which dominates during venous occulsion occurs globally across the forearm and thus, a diffuse variation in the reflectance response of forearm tissue is anticipated when venous outflow is restricted.

Next, we examine the spectral changes which accompany venous occlusion. The wavelengths between 400 and 1100 nm exhibit a general trend of increased attenuation over the venous occlusion time. Longer near infrared wavelengths display a higher intrinsic tissue attenuation but show a lesser response to venous occlusion than shorter near infrared wavelengths. This general increase in tissue attenuation across the visible and near infrared during venous occlusion is attributed to the increased blood volume. Greater blood volume results in a higher haemoglobin and water concentration in the optical path, resulting in an increased absorption in the spectral regions where haemoglobin and water dominate. In addition, the general increase in tissue attenuation also suggests that the scattering properties of the forearm are altered during venous occlusion. Changes in the tissue scatter function as a result of increased blood volume have previously not been considered when analysing the tissue attenuation during venous occlusion. However, our results suggest that this effect cannot be ignored.

A secondary characteristic of the venous occlusion protocol is the impaired venous washout which results in an increase in the accumulation of deoxygenated haemoglobin and various metabolites. The added attenuation at the deoxy-haemoglobin absorption maximum at 760 nm with venous occlusion time is indicative of metabolite accumulation and an associated decrease in the O_2 affinity of haemoglobin due to the increased CO_2 content of blood when the venous return of the blood is restricted. However, the subtle change in the tissue attenuation at 760 nm is largely over-shadowed by the effects of blood volume changes on the near infrared attenuation of tissue during venous occlusion. The pixel cluster membership maps of the near infrared reflectance time courses during the venous occlusion segment of the protocol cluster primarily on the blood volume changes associated with the restricted venous return of the blood and show little anatomical differentiation (see lower left panel of Fig. 8).

During complete forearm circulatory arrest (ischaemia), metabolites will accumulate locally without the accompanying increase in blood volume in the extremity. This provides the opportunity to map regional variations in attenuation of reflected near infrared light from the forearm without the confounding issue of varying blood volume. In contrast to venous occlusion, distinct regional variations appear over the forearm during the ischaemia protocol, and furthermore, this regional variation is wavelength dependent. In particular, forearm tissue attenuation at the long wavelength regions (> 800 nm) including the region of the water absorption maximum at 970 nm was generally uncorrelated with the ischaemia segment of the protocol. Clustering long wavelength reflectance image time-courses from the ischaemia segment of the protocol reveals little variation in tissue attenuation across the forearm during ischaemia and provides an additional indicator that

the blood volume in the optical path remained relatively constant throughout the ischaemia segment of the protocol.

The situation at 760 nm (Fig. 8) differs significantly from that observed at the longer near infrared wavelengths during ischaemia. At 760 nm, regions of the forearm at which the venous compartment dominates the near surface tissue correlate with the ischaemic response in peripheral tissues. Venous structures can be identified in the cluster map (see lower right panel in Fig. 8). The cluster associated with regions which have a high contribution from the venous compartment do not show a dramatic increase in attenuation at 760 nm during brief periods of ischaemia. However, tissues peripheral to these venous structures do display a marked increase in the attenuation of light at 760 nm during ischaemia. This suggests a significant local accumulation of deoxyhaemoglobin and a concomitant decrease in oxyhaemoglobin in these peripheral tissues resulting in an increased tissue absorption in the region of the deoxy-haemoglobin absorption maximum. It also suggests that under the condition of complete circulatory arrest, there is limited flow of deoxyhaemoglobin from peripheral tissue into the major venous structures: hence regions which are dominated by venous structures show little change in attenuation at 760 nm during complete ischaemia.

The above experiments illustrate some of the difficulties in developing a robust measure of blood volume changes based on the change in the near infrared attenuation of the target tissue. An increase in forearm blood volume leads to increased near infrared attenuation with the shortest wavelengths displaying the greatest change in attenuation. In addition, the attenuation over the shorter near infrared wavelength region is also sensitive to changes in tissue metabolism which affect haemoglobin oxygen saturation and the redox states of haemoglobin and cytochrome aa_3. Vasoactive responses which lead to a significant change in blood volume can also effect the status of tissue metabolism. Most near infrared investigations of blood volume changes attempt to accommodate for this lack of specificity in the attenuation response of tissue at the shorter near infrared wavelengths by measuring the attenuation at two or more wavelengths at which deoxy- and oxyhaemoglobin display a significant differential absorption. The combined response as determined by the absorption coefficients of deoxy- and oxyhaemoglobin at the measured wavelengths is related to the total haemoglobin concentration and thus the volume of blood in the optical path. This approach assumes that a change in tissue blood volume manifests itself as a change in near infrared absorption or at the very least that any change in the tissue scattering coefficient is wavelength independent over the range of wavelengths measured. However, if absorption is the sole contributor to the observed increase in the near infrared attenuation of tissue during an increase in blood volume, then, there should be an accompanying increase in the attenuation, localized in the region of the water absorption maxima, to account for the high water content in the volume of tissue. The small change in attenuation around 970 nm, the region of the water absorption maximum, which accompanies a change in blood volume suggests that the scattering may also be a significant contributer to the observed change in attenuation across the near infrared. Our results also suggest a wavelength dependent change in the tissue scatter function during blood volume changes. A reliable quantitative assessment of changes in blood volume and the rate of this change (blood flow) as well as the effects of changing hematocrit is hindered by the various origins and the complex interplay between the scattering and absorption contributions to the near infrared attenuation in tissues. To date, understanding this interplay between scattering and absorption remains the greatest challenge to developing near infrared spectroscopy as a quantitative tool for haemodynamic monitoring.

6. Conclusion

We have demonstrated that the interaction of infrared radiation with tissues and biological fluids results in characteristic absorptions that provide clinically relevant information. This information is sometimes purely qualitative, providing us with insights into the molecular nature of the disease process, on both a macroscopic and microscopic level. This qualitative information can often be converted non-subjectively into diagnostic information by the application of multivariate pattern recognition meth-

ods. Quantitative information can be extracted from IR spectra of biological fluids with relative ease, with a precision close to that of standard clinical chemistry methods. In addition, our initial work using near infrared spectroscopic imaging demonstrates that changes in blood flow, volume and oxygenation in peripheral tissue can be studied which may have applications in physiology and medicine. Almost a century after his death, Huxley's vision of "a means of making out the molecular structures of living tissues comparable to that which spectroscopy affords to the inquirer into the nature of the heavenly bodies" is a reality, in the form of medical infrared spectroscopy.

Acknowledgements

We wish to thank our colleagues in the Spectroscopy Group (Lin-P'ing Choo-Smith, Kan-Zhi Liu, James Mansfield, Christian Schultz, Anthony Shaw) and the Informatics Group (Rajmond Somorjai, Gordon Scarth and Alexander Nikhulin) of the Institute for Biodiagnostics and our clinical collaborators (Thomas Dembinski, William C. Halliday, James Johnston, Michael Leroux, Peter H. Watson).

References

[1] W. Herschel, Philos. Trans. R. Soc. London 90 (1800) 284.
[2] M. Melloni, Ann. Chim. Phys. 55 (1835) 337.
[3] A.J. Ångstrom, Reserches sur le spectre solaire, Paris (1868).
[4] S.P. Langley, Philos. Mag. 17 (1884) 194.
[5] W. Abney, R.E. Festing, Philos. Trans. 172 (1881) 887.
[6] R.N. Jones, Can. J. Spectrosc. 26 (1981) 1.
[7] E.K. Blout, R.C. Mellors, Science 110 (1949) 137.
[8] D.L. Woernley, Cancer Res. 12 (1952) 516.
[9] A. Elliot, E.J. Ambrose, Nature 165 (1950) 921.
[10] E.J. Ambrose, A. Elliot, Proc. R. Soc. London, Ser A 208 (1951) 75.
[11] S.N. Timasheff, H. Susi, L. Stevens, J. Biol. Chem. 242 (1967) 5467.
[12] H. Susi, Meth. Enzymol. 26 (1972) 445.
[13] W.K. Surewicz, H.H. Mantsch, Biochim. Biophys. Acta 952 (1988) 115.
[14] M. Jackson, H.H. Mantsch, CRC Crit. Rev. Biochem. Mol. Biol. 30 (1995) 95.
[15] D. Chapman, P. Byrne, G.G. Shipley, Proc. R. Soc. London, Ser. A 290 (1966) 115.
[16] R.L. Amey, D. Chapman, in: D. Chapman (Ed.), Biomembrane Structure and Function, MacMillan Press, London, 1983, p. 199.
[17] R. Mendelsohn, H.H. Mantsch, in: A. Watts, J.J.H.H. dePont (Eds.), Progress in Lipid–Protein Interactions, Vol. 2, Elsevier, Amsterdam, 1986, p. 103.
[18] H.H. Mantsch, R.N. McElhaney, Chem. Phys. Lipids 57 (1991) 213.
[19] M. Jackson, H.H. Mantsch, Spectrochim. Acta Rev. 15 (1993) 53.
[20] M. Tsuboi, K. Shuto, S. Higushi, Bull. Chem. Soc. Jpn. 41 (1968) 1821.
[21] E. Taillandier, J. Liqueir, J.A. Taboury, in: R.J.H. Clarke, R.E. Hester (Eds.), Advances in Infrared and Raman Spectroscopy (Advances in Spectroscopy, Vol. 12), Wiley, New York, 1985, p. 65.
[22] H. Eysel, M. Jackson, A. Nikhulin, R.L. Somorjai, G.T.D. Thomson, H.H. Mantsch, Biospectroscopy, in press.
[23] R.A. Shaw, S. Kotowich, H.H. Eysel, M. Jackson, G.T.D. Thomson, H.H. Mantsch, Rheumatol. Int. 15 (1995) 159.
[24] M.G. Sowa, H.H. Mantsch, Clacif. Tissue Int. 54 (1994) 481.
[25] H. Fabian, M. Jackson, L. Murphy, P.H. Watson, I. Fichtner, H.H. Mantsch, Biospectroscopy 1 (1995) 37.
[26] I.E. Frank, J.H. Kalivas, B.R. Kowalski, Anal. Chem. 55 (1983) 1800.
[27] L.-P. Choo, J.R. Mansfield, N. Pizzi, R.L. Somorjai, M. Jackson, W.C. Halliday, H.H. Mantsch, Biospectroscopy 2 (1995) 141.
[28] C.P. Schultz, M.K. Ahmed, C. Dawes, H.H. Mantsch, Anal. Biochem. 240 (1996) 7.
[29] C.P. Schultz, H.H. Eysel, H.H. Mantsch, M. Jackson, J. Phys. Chem. 100 (1996) 6845.
[30] R.A. Shaw, S. Kotowich, H.H. Mantsch, M. Leroux, Clin. Biochem. 29 (1996) 11.
[31] K.-Z. Liu, M.K. Ahmed, T.C. Dembinski, H.H. Mantsch, Int. J. Gynec. Obstetrics 57 (1997) 161.
[32] C.P. Schultz, K.-Z Liu, J.B. Johnston, H.H. Mantsch, Leukemia Res. 20 (1996) 649.
[33] M. Jackson, J.R. Mansfield, B. Dolenko, R.L. Somorjai, P.H. Watson, H.H. Mantsch, Cancer Detection and Prevention, in press.
[34] L.-P. Choo, D.L. Wetzel, W.C. Halliday, M. Jackson, S.L. Levine, H.H. Mantsch, Biophys. J. 71 (1996) 1672.
[35] J.P. Payne, J.W. Severinghaus, Pulse Oximetry, Springer-Verlag, 1986.
[36] L. Nicolai, Arch. Ges. Physiol. 229 (1932) 372.
[37] J.R. Squire, Clin. Sci. 4 (1940) 331.
[38] D.L. Drabkin, C.F. Schmidt, J. Biol. Chem. 157 (1945) 69.
[39] S. Nakajima, Y. Hirai, H. Takase, A. Kuse, S. Aoyagi, M. Kishe, K. Yamaguichi, Kokyu To Junkan 23 (1975) 709.
[40] M. Yelderman, W. New, Anesthesiology 59 (1983) 349.
[41] J.W. Severinghaus, J.F. Kelleher, Anesthesiology 76 (1992) 1018.
[42] J.A. Wahr, K.K. Tremper, Crit. Care Clinics 11 (1995) 199.
[43] N.B. Hampson, C.A. Piantadosi, J. Appl. Physiol. 64 (1988) 2449.

[44] A. Seiyama, O. Hazeki, M. Tamura, J. Biochem. 103 (1988) 419.
[45] R.A. De Blasi, M. Cope, M. Ferrari, Adv. Exp. Med. Biol. 317 (1992) 771.
[46] Y. Ozaki, T. Matsunaga, T. Miura, Appl. Spectrosc. 46 (1992) 180.
[47] R.A. De Blasi, M. Cope, C. Elwell, F. Safoue, M. Ferrari, Eur. J. Appl. Physiol. 67 (1993) 20.
[48] C.E. Elwell, M. Cope, A.D. Edwards, J.S. Wyatt, D.T. Delpy, E.O.R. Reynolds, J. Appl. Physiol. 77 (1994) 2753.
[49] R.A. De Blasi, M. Ferrari, A. Natali, G. Conti, A. Mega, A. Gasparetto, J. Appl. Physiol. 76 (1994) 1388.
[50] M.G. Sowa, J.R. Mansfield, G.B. Scarth, H.H. Mantsch, Appl. Spectrosc. 51 (1997) 43.
[51] J.R. Mansfield, M.G. Sowa, H.H. Mantsch, Comp. Med. Imag. Graph., in press.
[52] J.C. Bezdek, Pattern Recognition with Fuzzy Objective Function Algorithms, Plenum, New York, 1981.
[53] J.C. Bezdek, R. Ehrlich, W. Full, Comput. Geosci. 10 (1984) 191.